Journal of Physics D: Applied Physics

PAPER

Modelling cathode spots in glow discharges in the cathode boundary layer geometry

To cite this article: M S Bieniek *et al* 2016 *J. Phys. D: Appl. Phys.* **49** 105201

IOP Publishing

Journal of Physics D: Applied Physics

J. Phys. D: Appl. Phys. 49 (2016) 105201 (6pp)

doi:10.1088/0022-3727/49/10/105201

Modelling cathode spots in glow discharges in the cathode boundary layer geometry

M S Bieniek, P G C Almeida and M S Benilov

Departamento de Física, FCEE, Universidade da Madeira, Largo do Município, 9000 Funchal, Portugal
Instituto de Plasmas and Fusão Nuclear, IST, Universidade de Lisboa, Portugal

E-mail: mbieniek@uma.pt

Received 10 September 2015, revised 18 November 2015
Accepted for publication 30 November 2015
Published 3 February 2016

Abstract

Self-organized patterns of cathode spots in glow discharges are computed in the cathode boundary layer geometry, which is the one employed in most of the experiments reported in the literature. The model comprises conservation and transport equations of electrons and a single ion species, written in the drift-diffusion and local-field approximations, and Poisson's equation. Multiple solutions existing for the same value of the discharge current and describing modes with different configurations of cathode spots are computed by means of a stationary solver. The computed solutions are compared to their counterparts for plane-parallel electrodes, and experiments. All of the computed spot patterns have been observed in the experiment.

Keywords: self-organization, multiple solutions, dc glow microdischarges, cathode boundary layer, microdischarges, cathode spots

(Some figures may appear in colour only in the online journal)

1. Introduction

Self-organized patterns of cathode spots in DC glow microdischarges were observed for the first time in 2004 [1] and represent an important and interesting phenomenon. A range of experimental reports have since been published [1–10]. Modelling of the phenomenon [9, 11–15] has revealed, in agreement with the general theory of cathode spots and patterns in arc and DC glow discharges [16], the existence of multiple steady-state solutions for a given value of discharge current, which comprise modes of current transfer associated with different cathode spot patterns. Predictions concerning the existence of self-organized patterns in gases other than xenon, generated from the modelling, have been confirmed experimentally [9].

The vast majority of the experiments [1–10] have been performed in a discharge device comprising a flat cathode and a ring-shaped anode, separated by a dielectric (see e.g. figure 1 of [10]); this discharge configuration is called cathode boundary layer discharge (CBLD) by the authors of the experiment. However, the modelling has been performed up to date for discharges with parallel-plane electrodes only [9, 11–15]. The question of how the shape of the anode affects the pattern of self-organization has so far not been addressed. Furthermore, the effect over 3D spots of absorption of the charged particles by a dielectric surface has not been investigated in full due to computational difficulties [14].

In this work, 3D modelling of cathode spots is reported for the first time in CBLD, and the self-organization is computed with a full account of absorption of charged particles at the dielectric surface. The outline of the paper is as follows. The model is described in section 2. In section 3.1 the effect over the fundamental mode of the discharge radius, the thickness of the cathode and dielectric, and of a dielectric surface that reflects charged particles is investigated. In section 3.2 examples of computed 3D modes are given and compared to their experimental counterparts, the effect on 3D modes of a dielectric surface that reflects charged species is also analyzed. In section 4 conclusions are drawn.

2. Model and numerics

The model employed in this work is the most basic self-consistent model of glow discharge. Although the model is very well-known, it is described here for the sake of completeness.

The model comprises equations for conservation of electrons and a single ion species, written in the drift-diffusion transport approximation, and Poisson's equation:

$$\begin{aligned} \nabla\cdot\mathbf{J}_i &= n_e\,\alpha\,\mu_e\,E-\beta\,n_e\,n_i, \quad \mathbf{J}_i = -D_i\,\nabla n_i - n_i\,\mu_i\,\nabla\varphi, \\ \nabla\cdot\mathbf{J}_e &= n_e\,\alpha\,\mu_e\,E-\beta\,n_e\,n_i, \quad \mathbf{J}_e = -D_e\,\nabla n_e + n_e\,\mu_e\,\nabla\varphi, \\ \varepsilon_0\,\nabla^2\varphi &= -e\,(n_i-n_e). \end{aligned} \tag{1}$$

Here n_i, n_e, $\mathbf{J}_i$, $\mathbf{J}_e$, D_i, D_e, μ_i, and μ_e are number densities, charged species transport fluxes, diffusion coefficients, and mobilities of the ions and electrons, respectively; α is Townsend's ionization coefficient; β is coefficient of dissociative recombination; φ is electrostatic potential, $E=|\nabla\varphi|$ is electric field strength; ε_0 is permittivity of free space; and e is elementary charge. The local-field approximation is employed (i.e. electron transport and kinetic coefficients are assumed to depend on the local electric field only).

Boundary conditions at the cathode and anode are written in the conventional form. Diffusion fluxes of the attracted particles are neglected as compared to drift; the normal flux of the electrons emitted by the cathode is related to the flux of incident ions in terms of the effective secondary emission coefficient γ, which is assumed to characterize all mechanisms of electron emission (due to ion, photon, and excited atom bombardment) [17]; density of ions vanishes at the anode; electrostatic potentials of both electrodes are given. The dielectric surface is electrically insulating, and absorbs the charged particles (i.e. case *(i)*) $n_i=n_e=0$); for comparison, some solutions were computed for the case of a reflecting dielectric surface (i.e. case *(ii)*) $\frac{\partial n_i}{\partial r}=\frac{\partial n_e}{\partial r}=0$). With the computational domain from figure 1, the boundary conditions read

$$\begin{aligned} &\text{cathode } (AB): \quad \frac{\partial n_i}{\partial z}=0, \quad J_{ez}=-\gamma J_{iz}, \quad \varphi=0; \\ &\text{anode } (CDE): \quad n_i=0, \frac{\partial n_e}{\partial n}=0, \quad \varphi=U; \\ &\text{dielectric } (BC): \quad \begin{matrix} (i)\; n_i=n_e=0 \\ (ii)\dfrac{\partial n_i}{\partial r}=\dfrac{\partial n_e}{\partial r}=0 \end{matrix}, \quad J_{er}-J_{ir}=0; \\ &\text{numerical boundary (EFG)}: \quad n_i=n_e=0\,, \quad \frac{\partial\varphi}{\partial n}=0. \end{aligned} \tag{2}$$

Here U is the discharge voltage, the subscripts r and z denote radial and axial projections of corresponding vectors, and $\partial/\partial n$ means a normal derivative. The lengths DE and AG are large enough so that boundaries EF and FG do not affect the solution; simulations were run also with a smaller calculation domain (lengths DE and AG were reduced) and no significant differences in the solutions were observed. The results reported in this work refer to $h=0.5$ mm, $h_a=0.1$ mm, and $R=0.5$ mm unless indicated otherwise.

The control parameter can be either discharge voltage U or discharge current I, depending on the slope of the current voltage-characteristics (CVC) $U(I)$. In the first case, the value U of potential on the anode is set as the input parameter. In the second case, the problem is supplemented by a requirement that the discharge current takes a prescribed value and U is treated as an unknown that has to be found as a part of

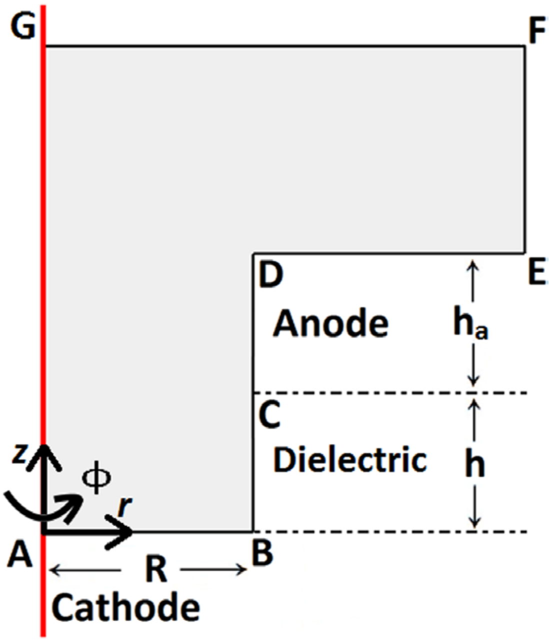

Figure 1. Configuration of a cathode boundary layer vessel. AG is the axis of symmetry of the vessel.

the solution; the calculation in this case is performed using a weak formulation in COMSOL Multiphysics.

Results reported in this work refer to a discharge in xenon under the pressure of 30 Torr. The (only) ionic species considered is Xe_2^+. The transport and kinetic coefficients are the same as in [14]. Note that a more detailed model (one that also took into account both atomic and molecular ions, excited atoms, excimers, stepwise ionization, ionization of excimers and non-locality of electron energy) was used for investigation of axially symmetric self-organized patterns in the parallel-plane configuration [14] and gave patterns qualitatively similar to those predicted by the relatively simple model described in this section. On the other hand, the simple model results in significantly reduced computation time, which was essential when performing 3D modelling. Therefore, the simple model was seen as adequate for the purpose of investigating the effect of CBL discharge configuration.

The problem (1)–(2) admits multiple solutions describing different discharge modes. One such mode exists for all ranges of current, it is 2D (axially symmetric) and termed fundamental, this is routine to calculate. 3D modes bifurcate from (and rejoin) the fundamental mode and are termed non-fundamental modes.

To calculate non-fundamental modes, one first locates points of bifurcation on the fundamental mode by means of linear stability analysis. The procedure is discussed in detail in [11] and in brief may be described as follows. Axially symmetric 2D stationary solutions are found for the problem (1)–(2) for a wide range of currents. Azimuthally periodic perturbations with an exponential time dependence are introduced. The time-dependent form of problem (1)–(2) is then linearized and assumes the form of an eigenvalue problem for a set of linear homogeneous differential equations, the perturbation increment λ being the eigenparameter. For each current

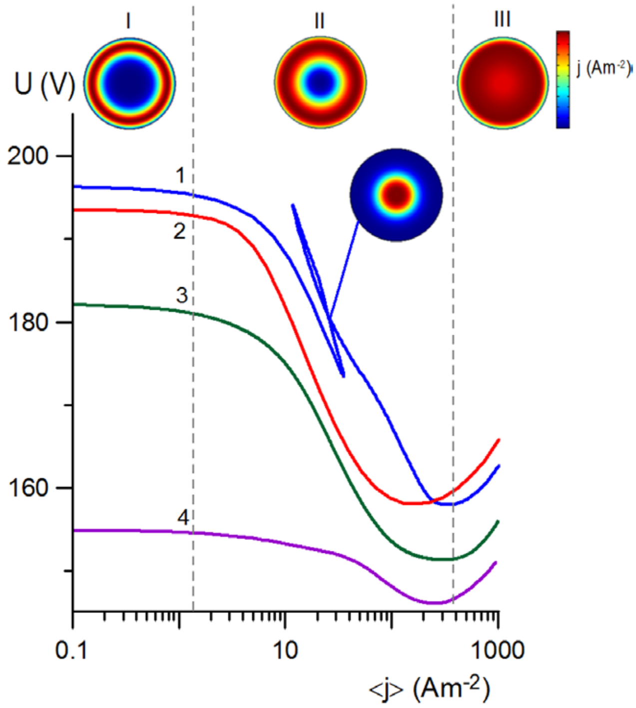

Figure 2. Fundamental mode. 1: baseline conditions. 2: $h = 0.5$ mm, $h_a = 0.1$ mm, $R = 1.5$ mm. 3: baseline geomentry, reflecting dielectric surface. 4: $h = 0.25$ mm, $h_a = 0.25$ mm, $R = 0.375$ mm.

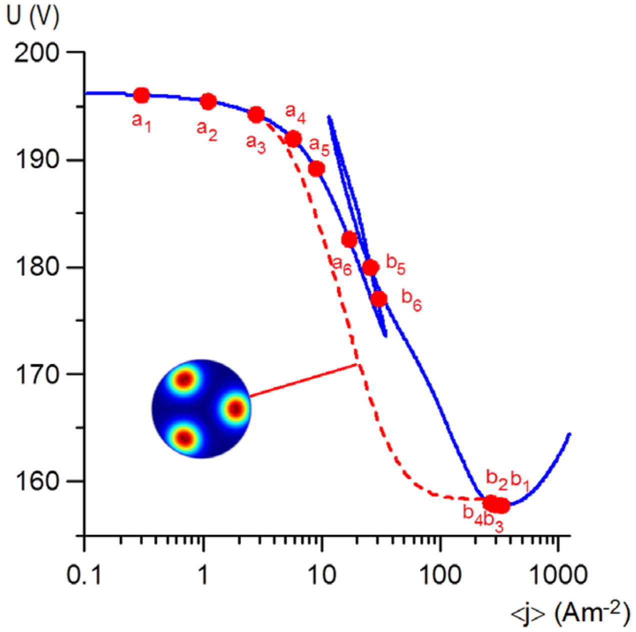

Figure 3. Solid: fundamental mode (mode 1 of figure 2). Dashed: mode a_3b_3. Circles: points of bifurcation.

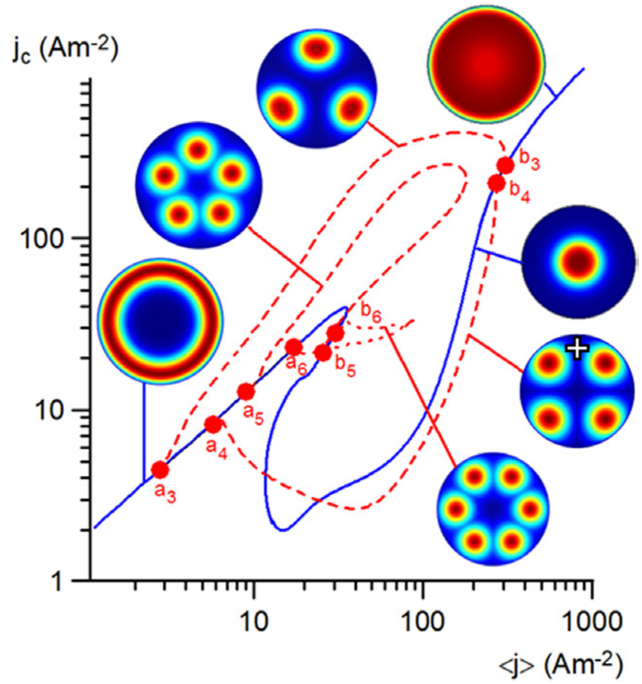

Figure 4. Bifurcation diagram. Solid: fundamental mode (mode 1 of figure 2). Dashed: modes a_3b_3, a_4b_4, a_5b_5. Dotted: mode a_6b_6. Circles: points of bifurcation. '+' on the image representing the mode a_4b_4 indicates the point on cathode surface where the value j_c is taken.

and each azimuthal period, the problem is solved by means of the eigenvalue solver of COMSOL Multiphysics. Bifurcations are found at currents where λ vanishes.

Next a 3D calculation domain is created by rotating the 2D domain *ABCDEFG* from figure 1 about the axis *AG* of symmetry of the discharge vessel, by an angle equal to half of the azimuthal period of the 3D mode being sought. The beginning of the non-fundamental mode is then searched for on the fundamental mode, with the 3D calculation domain, in the vicinity of the bifurcation point predicted by the linear stability analysis. Small azimuthally periodic perturbations are introduced to the densities of charged species at the bifurcation point; the stationary solver's iterations will eventually converge to the 3D mode. The remainder of the 3D mode is straightforward to calculate.

The above procedure was realized using stationary and eigenvalue solvers from the commercial product COMSOL Multiphysics. The meshes used were considered appropriate when after increasing their refinement the solutions were not significantly affected. The time taken by the stationary solver to find convergence to one of the most computationally intensive 3D solutions is around 1 h, with a computer with an Intel Core i7-4770 CPU at 3.4 GHz and 32 GB of RAM.

3. Results

3.1. Fundamental mode

In figure 2, the CVC of the fundamental mode is displayed in four sets of conditions, labeled 1–4 in the figure. Surprisingly, two turning points and a loop are present on the CVC corresponding to the baseline conditions ($h = 0.5$ mm, $h_a = 0.1$ mm, and $R = 0.5$ mm, absorbing dielectric surface), line 1.

The whole current range in figure 2 can be divided into three regions, marked I, II, III. At the top of the figure there is an illustration of the characteristic distribution of current density on the cathode surface for each region. The color range shown in the bar is used also for the rest of the document. The general pattern of evolution of the fundamental mode with

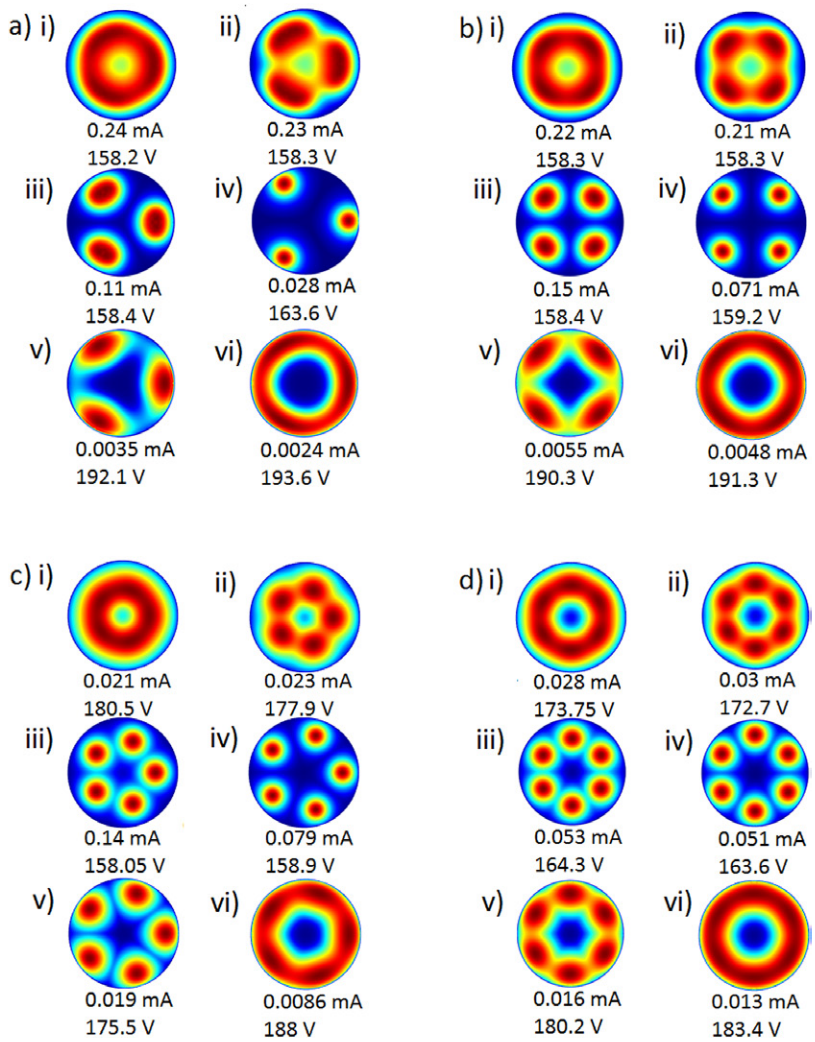

Figure 5. Evolution of patterns of current density on the cathode associated with 3D modes of figure 4: (a) mode a_3b_3, (b) mode a_4b_4, (c) mode a_5b_5 and (d) mode a_6b_6.

increasing current is as follows. In region I, corresponding to the Townsend discharge, the current is distributed on the cathode in the form of a ring. In region II, the ring of current grows thicker with increasing current. In region III, corresponding to the abnormal discharge, the discharge fills most of the cathode surface.

In the case represented by line 1, a pattern with a central spot appears on the section between the turning points, as indicated in the figure. This transition is accompanied by a loop in the CVC. The loop is absent in the CVC of cases 2 and 3; the larger radius and the reflecting dielectric surface, respectively, prevent the transition from a ring to central spot. The loop is also absent in the CVC of case 4. The CVC of cases 1, 2 and 4 (the ones with absorbing dielectric surface) have small humps in range I, although this cannot be seen in the scale of figure 2.

3.2. 3D modes

Figure 3 displays the CVC of the fundamental mode for the baseline conditions, points of bifurcation of 3D modes, and an example 3D mode. Each pair of points a_i and b_i designates from where a 3D mode branches off from and rejoins the fundamental mode. Mode a_ib_i possesses period $2\pi/i$, meaning that a_1b_1 possesses azimuthal period 2π, mode a_2b_2 possesses azimuthal period π, and so on. Bifurcation points b_1 to b_4 virtually coincide. Points b_5 and b_6 are positioned on the section between the turning points. The 3D modes branch off and rejoin the fundamental mode in a palindromic order along current, which conforms to previous modelling of discharges with parallel-plane electrodes.

As an example, the CVC of mode a_3b_3 is shown in figure 3. (The schematic in the figure illustrates the pattern of spots associated with this mode.) The CVC manifests a plateau between 60 A m^{-2} and 300 A m^{-2}, which is a manifestation of the normal current density effect. Note that the plateau also is present in the computed mode of the same azimuthal period for a vessel with parallel-plane electrodes and reflecting dielectric surface [15].

CVCs of several different modes would be difficult to distinguish in figure 3. A more convenient representation is shown in figure 4: the fundamental and four non-fundamental

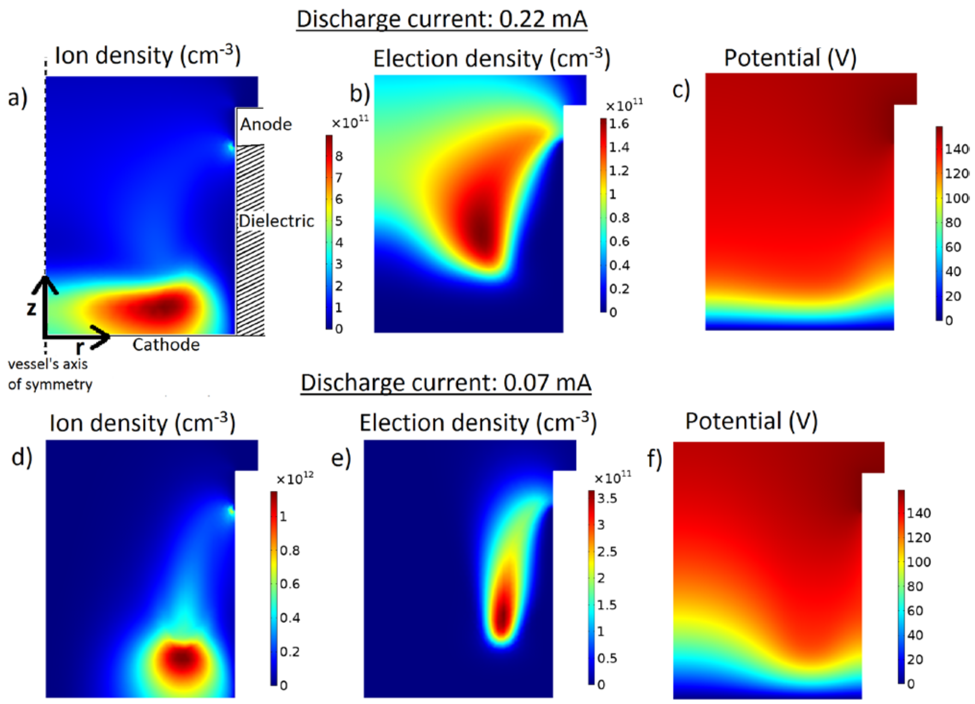

Figure 6. Cross section view of a 3D hot spot associated with the mode a_4b_4 at different currents. The cross section plane passes through the centre of the spot. (a), (d): Ion density. (b), (e): Election density. (c), (f): Potential.

modes are mapped in the plane $(\langle j\rangle, j_c)$, where $\langle j\rangle$ is the average current density on the cathode and j_c is the value of current density at the position $r = 0.4$ mm on the upper vertical radius as marked by a cross on one of the images in figure 4. Note that the value $r = 0.4$ mm coincides with the radius of the ring associated with the fundamental mode in the Townsend regime; it was found that such a choice ensures maximum distinction between the modes. Following the fundamental mode from low to high currents, it is seen that j_c decreases while the central spot is forming, then it increases as the ring mode forms, thus yielding a limp *Z*-shape on the bifurcation diagram. Modes a_5b_5, a_6b_6 possess turning points.

In figure 5 the evolution is shown of patterns of current density on the cathode associated with modes a_3b_3, a_4b_4, a_5b_5, a_6b_6 from figure 4 as discharge current is changed. Let us consider first the evolution of the patterns for mode a_3b_3 which is shown in figure 5(a). The state (a)(i) is positioned in the vicinity of the bifurcation point b_3, the pattern is of three diffuse elongated spots, slightly deforming into a structure with the period of $2\pi/3$. At (a)(ii) the three spots have become more distinct, intense and bean-shaped. The spots then become circular, and move farther from the center of the cathode as seen in state (a)(iv). The spots then once more become bean-shaped, then once again gain a triangular type structure as in state (a)(v). At state (a)(v) a central triangle-shaped 'cold spot' is present. Continuing along the mode with decreasing current, the triangle shaped region becomes less sharp, and the whole pattern becomes more like the ring-shaped distribution present at a_3.

The evolution of the patterns associated with modes a_4b_4, a_5b_5, and a_6b_6, is shown in figures 5(b)–(d), respectively, follows the same trend as mode a_3b_3: first the ring is transformed into elongated bean-shaped spots and then circular spots, then they migrate to a different radius, and there, from circular spots they turn into bean-shaped spots and then merge into a different ring. No 3D modes with central hot spots were found in the present work, while in previous modelling they were; e.g. [15]. The images in figure 5 can be compared to experimentally observed patterns of spots, figure 2 of [10]. The computed evolution from the abnormal mode into mode a_4b_4, comprising four spots (figure 5(b)), is in good agreement with the experimentally observed transition between the abnormal mode into a mode comprising four spots.

In figure 2 of [10], it can be seen how the modes appear in the experiment: starting from the abnormal mode and reducing discharge current, a mode comprising four spots appears. As current is further reduced, modes comprising five and six spots appear. Further reducing current from the mode with six spots, the discharge goes back to modes with five, four, three and a ring spot. In the modelling, see figure 3, starting from a state in the abnormal mode and following the fundamental mode in the direction of low currents, the bifurcation point b_1 of mode a_1b_1, comprising one spot, appears first. The next bifurcation point to appear is b_2 of mode a_2b_2, comprising two spots; and so on until bifurcation point b_6 of mode a_6b_6, comprising six spots, following the same trend observed in the experiment. On further following the fundamental mode in the direction of low currents, eventually the bifurcation point a_5 of mode a_5b_5 appears; and so on until a_1 of mode a_1b_1, again following the same trend as in the experiment.

In figure 6, typical distributions of discharge parameters along a cross section of a hot spot are shown. Figures 6(a)–(c) refer to state (i) in figures 5(b) and 6(d)–(f) refer to state (iv). The effect of normal current density is seen in figures 6(a) and (c).

The patterns of current density on the cathode shown in figures 3–5 are essentially the same as in simulations for plane-parallel electrode configurations; e.g. figure 5 of [15]. The difference is that the spots in figure 5 of [15] are centred at the periphery of the cathode, while the 3D spots of the present work are centred and formed totally within the cathode. The latter is what is observed in the experiments [1–10]. The reason of this difference is in different boundary conditions at the dielectric surface: while modelling [15] has been performed for the reflecting surface (boundary condition (ii) in the third line of equation (2)), the 3D spots reported in the present work have been computed for the absorbing surface (boundary condition (i)). Unsurprisingly, the assumption of absorbing dielectric surface, being more realistic by itself, gives results with better agreement with the experiment.

4. Conclusions

Self-organized 3D spot modes are reported for a typical configuration of cathode boundary layer discharge ($h = 0.5\,\mathrm{mm}$, $h_a = 0.1\,\mathrm{mm}$, and $R = 0.5\,\mathrm{mm}$) in xenon at the pressure of 30 Torr. The general form of the computed self-organized patterns is similar to those computed previously in the parallel-plane configuration and to those observed in the experiment in the sense that all of them comprise axially symmetric ring spots or circular arrangements of 3D spots. This is consistent with experimental evidence [4] that similar self-organized patterns appear in both electrode configurations.

Simulations of 3D spot patterns with the dielectric surface fully absorbing the charged particles reveal spots not centered at the periphery of the cathode, but rather located inside the cathode, as they are in the experiment. It has been found that there is a palindromic series of the number of spots with discharge current, which is consistent with observations of switching between modes with different patterns in the experiment [10].

Acknowledgments

The work was supported by FCT—Fundação para a Ciência e a Tecnologia of Portugal through the projects PTDC/FIS-PLA/2708/2012 and Pest-OE/UID/FIS/50010/2013.

References

[1] Schoenbach K H, Moselhy M and Shi W 2004 *Plasma Sources Sci. Technol.* **13** 177
[2] Moselhy M and Schoenbach K H 2004 *J. Appl. Phys.* **95** 1642
[3] Takano N and Schoenbach K H 2006 *Plasma Sources Sci. Technol.* **15** S109
[4] Takano N and Schoenbach K H 2006 *Abstracts of the 2006 IEEE Int. Conf. on Plasma Science (IEEE Traverse City, MI, USA)* p 247
[5] Lee B-J, Rahaman H, Frank K, Mares L and Biborosch D-L 2007 *Proc. 28th ICPIG (Prague, July 2007)* ed J Schmidt *et al* (Prague: Institute of Plasma Physics) pp 900–2
[6] Zhu W, Takano N, Schoenbach K H, Guru D, McLaren J, Heberlein J, May R and Cooper J R 2007 *J. Phys. D: Appl. Phys.* **40** 3896
[7] Lee B-J, Biborosch D-L, Frank K and Mares L 2008 *J. Optoelectron. Adv. Mater.* **10** 1972
[8] Schoenbach K H and Zhu W 2012 *IEEE J. Quantum Electron.* **48** 768
[9] Zhu W, Niraula P, Almeida P G C, Benilov M S and Santos D F N 2014 *Plasma Sources Sci. Technol.* **23** 054012
[10] Zhu W and Niraula P 2014 *Plasma Sources Sci. Technol.* **23** 054011
[11] Almeida P G C, Benilov M S, Cunha M D and Faria M J 2009 *J. Phys. D: Appl. Phys.* **42** 194010
[12] Almeida P G C, Benilov M S and Faria M J 2010 *Plasma Sources Sci. Technol.* **19** 025019
[13] Almeida P G C, Benilov M S and Faria M J 2011 *IEEE Trans. Plasma Sci.* **39** 2190
[14] Almeida P G C and Benilov M S 2013 *Phys. Plasmas* **20** 101613
[15] Almeida P G C, Benilov M S and Santos D F N 2014 ArXiv e-prints arXiv:1406.4394
[16] Benilov M S 2014 *Plasma Sources Sci. Technol.* **23** 054019
[17] Raizer Yu P 1991 *Gas Discharge Physics* (Berlin: Springer)